Study of deep traps in AlGaN/GaN high-electron mobility transistors by electrical characterization and simulation

Philippe Ferrandis, Mariam El-Khatib, Marie-Anne Jaud, Erwan Morvan, Matthew Charles, Gérard Guillot, Georges Bremond

Journal of Applied Physics

Study of deep traps in AlGaN/GaN high-electron mobility transistors by electrical characterization and simulation

Cite as: J. Appl. Phys. **125**, 035702 (2019); https://doi.org/10.1063/1.5055926
Submitted: 12 September 2018 . Accepted: 01 January 2019 . Published Online: 16 January 2019

Philippe Ferrandis, Mariam El-Khatib, Marie-Anne Jaud, Erwan Morvan, Matthew Charles, Gérard Guillot, and Georges Bremond

Journal of Applied Physics ARTICLE scitation.org/journal/jap

Study of deep traps in AlGaN/GaN high-electron mobility transistors by electrical characterization and simulation

Cite as: J. Appl. Phys. **125**, 035702 (2019); doi: 10.1063/1.5055926
Submitted: 12 September 2018 · Accepted: 1 January 2019 ·
Published Online: 16 January 2019

Philippe Ferrandis,[1,2,a)] Mariam El-Khatib,[3] Marie-Anne Jaud,[2] Erwan Morvan,[2] Matthew Charles,[2] Gérard Guillot,[3] and Georges Bremond[3]

AFFILIATIONS

[1]Université de Toulon, Aix Marseille Univ., CNRS, IM2NP, Toulon, France
[2]Univ. Grenoble Alpes, CEA, LETI, 38000 Grenoble, France
[3]Univ. de Lyon, Institut des Nanotechnologies de Lyon, CNRS UMR 5270, INSA de Lyon, Bât. Blaise Pascal, 7 avenue Jean Capelle, F-69621 Villeurbanne Cedex, France

[a)]E-mail: philippe.ferrandis@univ-tln.fr

ABSTRACT

The localization of deep traps in normally-off AlGaN/GaN metal-oxide-semiconductor channel high-electron mobility transistors has been established by means of capacitance and current deep level transient spectroscopies (DLTS). Electrical simulations of the total current density between the drain and source contacts, the electron density, and the equipotential line distribution helped to understand the transport mechanisms into the device and to determine the zone probed by DLTS measurements. By changing the drain-source voltage in current DLTS or the reverse bias in capacitance DLTS, we demonstrated that we can choose to probe either the region below the gate or the region between the gate and drain electrodes. We could then see that defects related to reactive ion etching induced surface damage, expected to be formed during the gate recess process, were located only under the gate contact whereas native defects were found everywhere in the GaN layer. Thanks to this method of localization, we assigned a trap with an $E_C - 0.5$ eV to ion etching induced damage.

I. INTRODUCTION

Thanks to its high electric breakdown field, high electron mobility, and high saturated electron velocity, GaN material has been employed for converters at higher frequencies and efficiencies than those achievable with conventional Si devices.[1] For AlGaN/GaN, several architectures have been proposed, including normally-off metal-oxide-semiconductor channel high-electron mobility transistors (MOSC-HEMTs) whose positive threshold voltage satisfies the requirement to be fail-safe.[2,3]

Despite numerous improvements of GaN power components during the last few decades, charge trapping effects at deep levels still prevent the reduction of the dynamic on-resistance and switching losses.[4–6] To detect these deep traps and determine in which part of the device structure they are located, capacitance deep level transient spectroscopy (C-DLTS) was applied to GaN Schottky barrier diodes.[7–10] In devices with small gate dimensions, where the capacitance is too weak to allow C-DLTS measurements, current-mode DLTS (I-DLTS) has been used.[11,12]

In this work, we made a comparative study of deep traps using C-DLTS and I-DLTS applied to an AlGaN/GaN MOSC-HEMT. The two modes of transient spectroscopy allowed localization of certain defects in the device, and the simulations of the total current density, the electron density, and the equipotential line distribution enabled clearer interpretation.

II. EXPERIMENTAL METHODS

MOSC-HEMTs were fabricated on structures grown by metalorganic chemical vapor deposition (MOCVD) on 200 mm

diameter Si(111) substrates. The epitaxial structure consists of an AlN nucleation layer, followed by AlGaN based buffer layers, then a 1.8 μm thick semi-insulating carbon doped GaN buffer layer, a p-type GaN back barrier used to confine carriers into the channel, an unintentionally doped (UID) GaN layer acting as the channel, a 1 nm unintentionally doped AlN layer, and a 21.4 nm unintentionally doped $Al_{0.20}Ga_{0.80}N$ barrier layer. Si_3N_4 was used for the top passivation. More details on the epitaxial layer stack can be found elsewhere.[13] Interdigitated comb-like transistor structures were used, with fingers 1000 μm long and 11 μm wide for both source and drain contacts. The gate electrode was formed by 100 fingers which were 1000 μm long and 1 μm wide, giving a surface area of 100×10^3 μm^2. The gate metal was formed using TiN/W, and the source and drain ohmic contacts were Ti/Al. The recessed gate electrodes were produced by etching the Si_3N_4 passivation and 35 nm of the AlGaN/GaN bilayer using a low bias chlorine (Cl_2/BCl_3) Inductively Coupled Plasma (ICP) – Reactive Ion Etching (RIE) etching process. To form the gate oxide, 30 nm of Al_2O_3 was deposited at 300 °C using atomic layer deposition with $Al(CH_3)_3/H_2O$ precursors. The gate-to-drain and gate-to-source distances were $L_{gd} = 15\,\mu$m and $L_{gs} = 2\,\mu$m, respectively.

Deep level transient spectroscopy data were acquired with a Fourier transform deep level transient spectroscopy system from PhysTech (FT 1030) using a Boonton 72B capacitance meter with a 100 mV test signal at 1 MHz. Capacitance and current transients were recorded between 80 K and 450 K in the warm up mode.

Drift-diffusion electrical simulations of MOSC-HEMTs were performed using the Synopsys S-Device module.[14] The simulated structure was composed of a 1 nm AlN with a 21.4 nm thick AlGaN barrier containing 20% aluminum, a 30 nm of Al_2O_3 gate insulator, a 40 nm thick Si_3N_4 passivation layer, and a p-type GaN back barrier. The piezoelectric polarization strain model with Vurgaftman values[15] was used to calculate the piezo-polarization effect. A mobility model including phonon scattering [with $\mu max = 1500\ cm^2\,(V\,s)^{-1}$ for electron in GaN] and a doping dependent mobility degradation was assumed.

III. CAPACITANCE DLTS AND SIMULATIONS

Voltage pulses were applied to the gate contact, and capacitance transients were recorded between the gate and drain electrodes. In Fig. 1, the C-DLTS spectrum of a MOSC-HEMT is reported with a reverse bias $V_R = 0$ V, a filling pulse height $V_P = 2$ V, a filling pulse width $t_P = 1$ ms, and a period width $T_W = 200$ ms. A capacitance-voltage measurement carried out at 300 K between the gate and drain electrodes exhibits a pinch-off voltage of 0 V. According to this value, the probed zone related to C-DLTS data depicted in Fig. 1 is located in the unintentionally doped GaN channel layer where the two-dimensional electron gas (2DEG) forms. Three electron traps clearly appear in the spectrum, labeled E2, E4, and E5. A fourth electron trap, called E6, appears as a high-temperature shoulder on E5. These labels are the same as those used in a previous work where an identification of traps was proposed.[13] E2 has an activation enthalpy $E_T = 0.31$ eV and capture cross section $\sigma_T = 3.9 \times 10^{-15}$ cm^2 and is related to reactive ion etching induced surface damage.[16,17] This trap appears during the ion-assisted gate recess process[18] and so is coherent with this interpretation. E4 has an activation enthalpy $E_T = 0.5$ eV and capture cross section $\sigma_T = 8 \times 10^{-14}$ cm^2 and has not been clearly identified. It could be related to carbon according to certain work in the literature.[19,20] The presence of a low density of carbon atoms in the unintentionally doped GaN layer could be due to an intrinsic carbon incorporation occurring during MOCVD growth since the gallium precursor (trimethylgallium) contains methyl groups. However, a trap with $E_T = 0.5$ eV has also been associated with GaN HEMT degradation during stress experiments.[21–23] Thus, trap E4 could also be linked to dry etching induced surface damage because defects formed during electron, proton, or ion irradiation are assumed to be jointly associated with nitrogen vacancies.[24] Trap E5 has an activation enthalpy $E_T = 0.64$ eV and capture cross section $\sigma_T = 1.2 \times 10^{-14}$ cm^2, and trap E6 has an activation enthalpy $E_T = 0.79$ eV and capture cross section $\sigma_T = 5 \times 10^{-15}$ cm^2. These are native defects related to gallium vacancies[7,25–29] and interstitial nitrogen,[30,31] respectively.

In Fig. 1, we see that trap E5 dominates the spectrum with a maximum amplitude of 0.21 pF. By changing the reverse bias to $V_R = -10$ V, the probed zone is changed (Fig. 2) and trap E6 becomes dominant despite an increase of the amplitude for trap E5 to 0.8 pF.

Electrical simulations of the electron density and the equipotential line distribution in a MOSC-HEMT at $V_R = 0$ V and $V_R = -10$ V are shown in Fig. 3. We see that the depleted region is centered below the gate electrode in the unintentionally doped GaN layer for $V_R = 0$ V but extends below the field plates for $V_R = -10$ V. Moreover, with $V_R = -10$ V no equipotential lines appear beneath the gate electrode between the interface with Al_2O_3 and the carbon doped GaN buffer

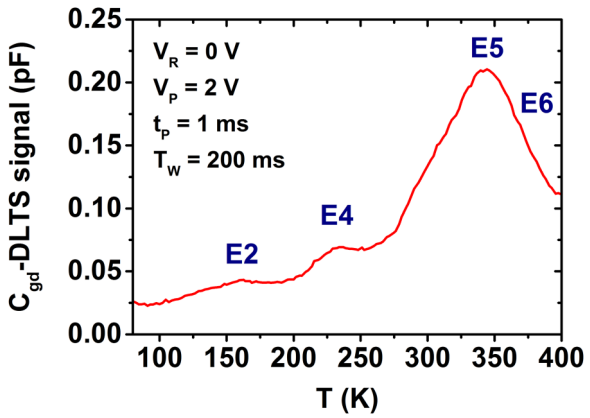

FIG. 1. C-DLTS spectrum of a MOSC-HEMT recorded between the gate and drain electrodes with a reverse bias $V_R = 0$ V.

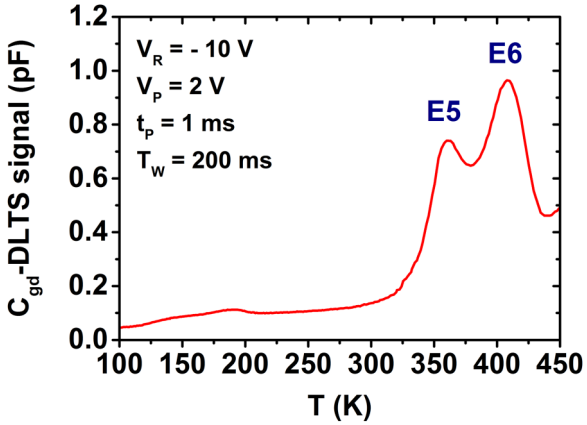

FIG. 2. C-DLTS spectrum of a MOSC-HEMT recorded between the gate and drain electrodes with a reverse bias $V_R = -10$ V.

layer. This means that the GaN conduction band minimum is constant in the region covered by the unintentionally doped GaN layer and the p-GaN back barrier. Consequently, we believe that electrons released by the thermal energy in this region are not deported due to the absence of electric field, and hence they do not participate in transients which give a C-DLTS signal.

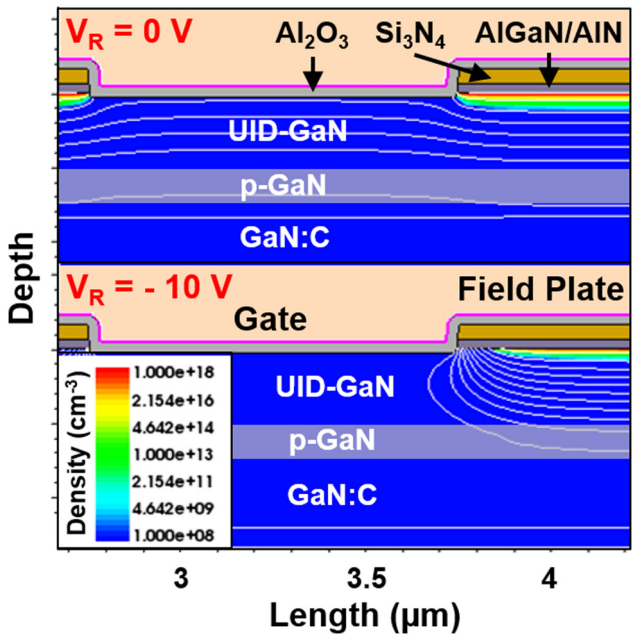

FIG. 3. Electrical simulations of the electron density and the equipotential line distribution in a MOSC-HEMT at $V_R = 0$ V and $V_R = -10$ V.

For a reverse bias $V_R = 0$ V (Fig. 1), the region investigated by C-DLTS is centered beneath the gate and we see traps E2, E4, E5, and E6. When the reverse bias is $V_R = -10$ V (Fig. 2), the probed region is mainly located below the field plates and extends deeper into the unintentionally doped GaN layer. Traps E5 and E6 increase in intensity compared to traps E2 and E4, suggesting that traps E2 and E4 are localized under the gate. As the GaN region without etching induced damage is favored with $V_R = -10$ V, native defects should dominate the spectrum. Consequently, trap E4 which seems not homogenously distributed in the unintentionally doped GaN layer cannot be associated with a native defect or a contamination by an impurity like carbon. Since the MOSC-HEMT used for this study did not undergo a stress, an association of trap E4 with stress-induced degradation is not expected.

IV. CURRENT DLTS AND SIMULATIONS

Figure 4 reports I-DLTS spectra of a MOSC-HEMT recorded between the source and drain electrodes with $V_{ds} = 1$ V, 3 V, and 5 V. For each measurement, the reverse bias and the filling pulse height applied to the gate contact were $V_R = 0.5$ V and $V_P = 3$ V, respectively. A filling pulse width $t_P = 1$ ms and a period width $T_W = 200$ ms were used for all spectra. With $V_{ds} = 1$ V, traps E2 and E4 dominate while trap E5 is just emerging. When V_{ds} increases all traps grow but not in the same proportion, as can be seen in Fig. 5. The ratio between the amplitudes of traps E5 and E2 or E4 is around 20% at $V_{ds} = 1$ V and stabilizes close to 70% as V_{ds} raises. The correspondence between traps determined by C-DLTS and I-DLTS has been confirmed by Arrhenius plots shown in Fig. 6.

Simulations of the total current density in a MOSC-HEMT with $V_{gs} = 0.5$ V and various V_{ds} are reported in Fig. 7. For $V_{ds} = 1$ V, we observe that the total current density is mainly

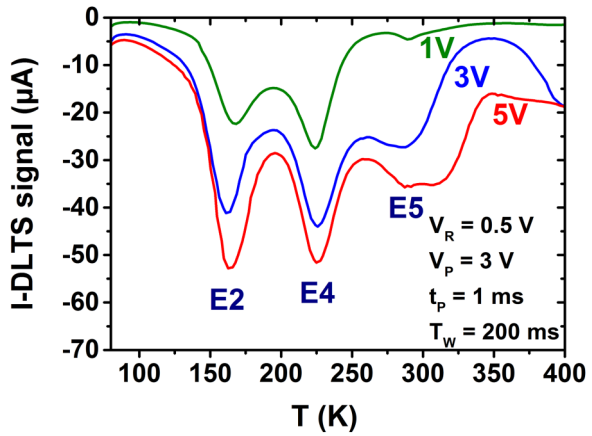

FIG. 4. I-DLTS spectra of a MOSC-HEMT recorded between the source and drain electrodes with a reverse bias $V_R = 0.5$ V applied to the gate contact. The drain-source electric potential differences (1 V, 3 V, and 5 V) are written down for each spectrum.

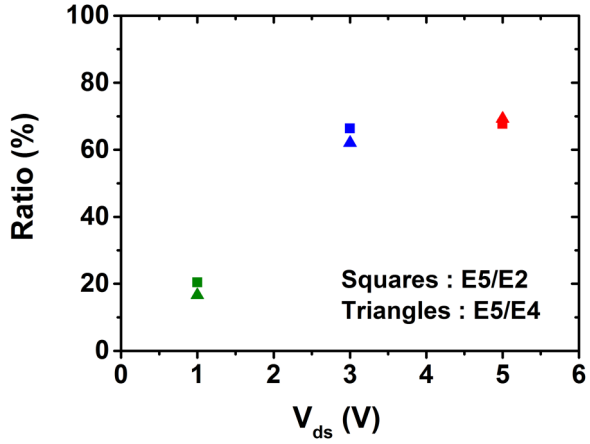

FIG. 5. Trap amplitude ratio between traps E5 and E2, and traps E5 and E4 as a function of V_{ds}. Data are extracted from I-DLTS spectra in Fig. 4.

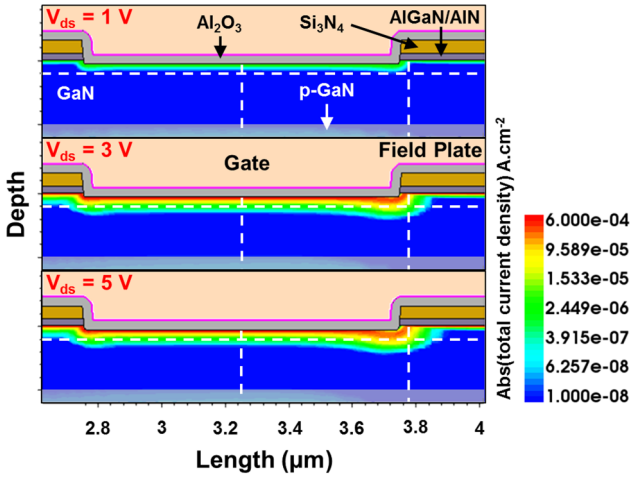

FIG. 7. Two-dimensional simulation of the total current density below the gate of a MOSC-HEMT for $V_{gs} = 0.5$ V and different V_{ds}. The source and drain electrodes are at the left and the right side of this schematic, respectively.

located close to the AlN/GaN heterojunction and is nearly homogeneously distributed beneath the gate electrode. As soon as V_{ds} reaches 3 V, the total current density increases at the vicinity of the edges of the gate and extends below the field plates. This extension is favored toward the drain side and the total current density remains concentrated in the unintentionally doped GaN layer.

The one-dimensional distribution of the simulated total current density along a line located 40 nm below the AlN/GaN interface can be seen in Fig. 8. Since the recessed gate was formed by etching to a depth of 12.6 nm into the GaN, this line is 27.4 nm under the gate. It is clear that the total current density is higher below the gate with two peaks of larger values close to the edges. By increasing V_{ds} from 1 V to 3 V or 5 V, the total current density raises everywhere along the line. It is important to notice from Fig. 9 that for $V_{gs} = 0.5$ V, the simulated drain current is in the increasing part of the characteristic with 5.8×10^{-12} A cm^{-1} at $V_{ds} = 1$ V, whereas it reaches the saturation regime with 6.9×10^{-10} A cm^{-1} and 7.1×10^{-10} A cm^{-1} at $V_{ds} = 3$ V and $V_{ds} = 5$ V, respectively. Moreover, we remark in Fig. 8 that for $V_{ds} = 3$ V or 5 V, the amplitude of the peak at the drain side is much higher than that at the source side.

In Fig. 10, the evolution of the simulated total current density along two cross sections (white vertical dashed lines

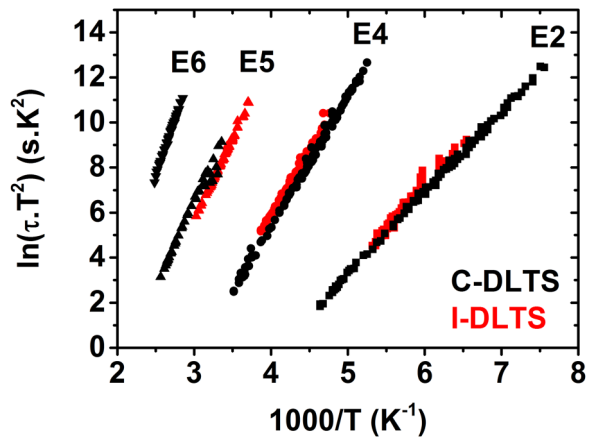

FIG. 6. Arrhenius plots extracted from C-DLTS and I-DLTS data for traps E2, E4, E5, and E6.

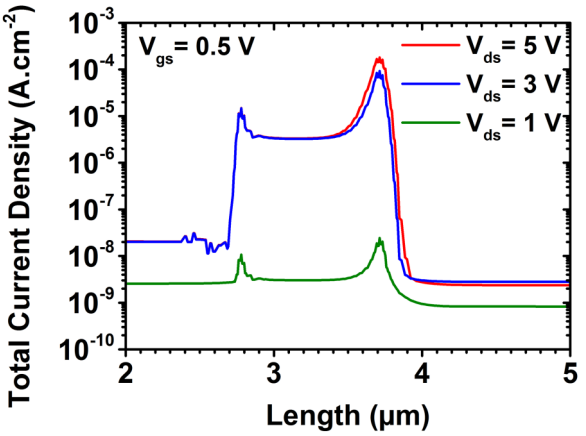

FIG. 8. One-dimensional distribution of the simulated total current density along a line (white horizontal dashed line in Fig. 7) located 40 nm below the AlN layer of a MOSC-HEMT for different V_{ds}.

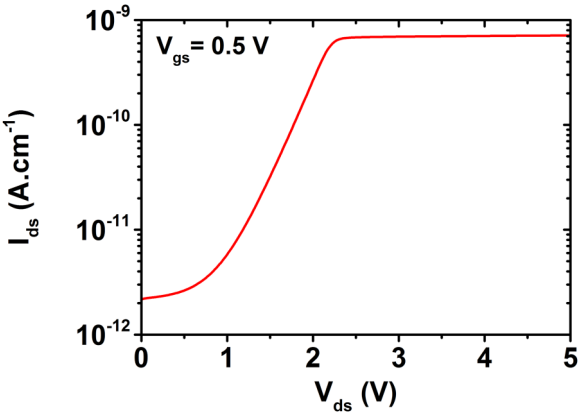

FIG. 9. Simulated drain current versus drain voltage for V_{gs} = 0.5 V.

in Fig. 7) located below the middle of the gate and below the field plate at the drain side confirms the previous conclusions. The simulations of the total current density demonstrate that with V_{ds} = 1 V, the region investigated by I-DLTS measurements is mainly localized below the gate. By increasing V_{ds}, the probed zone is extended into the unintentionally doped GaN layer. This extension occurs further beneath the field plates and is more significant at the drain side. Consequently, at V_{ds} = 1 V it is expected that defects located below the gate dominate the I-DLTS spectra whereas for larger V_{ds}, defects located under the field plates should significantly compete with defects which lie just below the gate. In addition, the integrated total current density as a function of the depth is

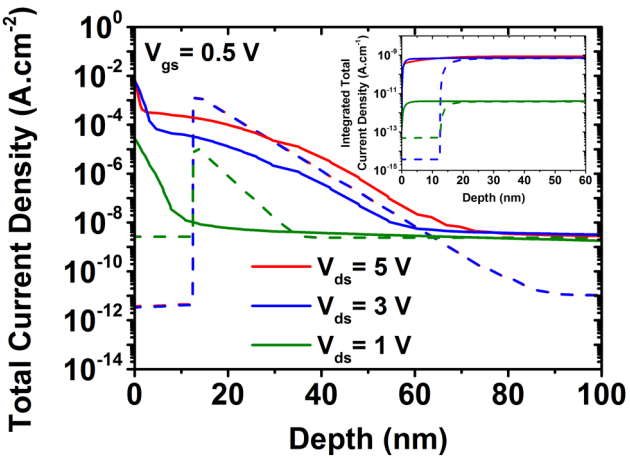

FIG. 10. One-dimensional distribution of the simulated total current density along two cross sections (white vertical dashed lines in Fig. 7) located below the middle of the gate (dashed curves) and below the field plate at the drain side (solid curves) for different V_{ds}. The inset depicts the integrated total current density versus the depth along the two vertical cross sections.

depicted in the inset of Fig. 10. For each V_{ds}, the convergence of the dashed and solid curves to the same value when the depth is larger than 20 nm demonstrates that the total current density remains constant throughout the channel.

In Fig. 4, we clearly see that traps E2 and E4 are present on all spectra, while trap E5 is nearly unobservable at V_{ds} = 1 V and increases for larger V_{ds} with an amplitude which follows that of traps E2 and E4. Therefore, we conclude that traps E2 and E4 are located beneath the gate, whereas trap E5, which is a native defect, is uniformly distributed in the GaN layer. This conclusion is consistent with the nature of trap E2. Being related to the ion-assisted gate recess process, this defect is expected to be localized only under the etched GaN region. Furthermore, in view of these findings, we can assume that trap E4 is also associated with a defect related to etching induced damage.

The same origin and location of traps E2 and E4 could explain the similar behavior of these traps in Fig. 5. Additionally, we note in Fig. 9 that the drain current saturates above V_{ds} = 3 V. This means that the quantity of charge collected by the drain electrode shows no further change above V_{ds} = 3 V. In Fig. 8, the total current density does not significantly change between V_{ds} = 3 V and V_{ds} = 5 V, which results in a weak extension of the probed region above V_{ds} = 3 V. The saturation of the drain current and the low modification of the investigated zone for V_{ds} larger than 3 V are responsible for the saturation of the trap amplitude ratio in Fig. 5.

V. CONCLUSION

Capacitance and current DLTS measurements assisted by electrical simulations were applied to MOSC-HEMT structures. The simulations of the total current density have demonstrated that the region investigated by I-DLTS can be changed depending on V_{ds} values. Furthermore, we found that the probed zone is also modified by changing the reverse bias in C-DLTS measurements. Consequently, two traps E2 and E4 have been localized below the gate. E2 is related to etching induced damage and is believed to be formed during the ion-assisted gate recess process. E4, with an activation enthalpy of 0.5 eV, is also assumed to be associated with a defect related to etching induced damage. Two other traps E5 and E6, associated with native defects, have been found everywhere in the unintentionally doped GaN channel layer. The combination of the electrical simulations and DLTS characterizations proves that the tuning of the measurement parameters allows us to find the position of defects within the channel of MOSC-HEMT. This method is powerful to discriminate between native defects and traps formed by technological steps.

ACKNOWLEDGMENTS

This work was funded by the French national program "programme d'Investissements d'Avenir, IRT Nanoelec" ANR-10-AIRT-05 and was supported by a doctoral fellowship (ADR to M. El-Khatib) from the "Région Auvergne-Rhone-Alpes" via the "ARC4."

REFERENCES

[1]E. A. Jones, F. Wang, and D. Costinett, IEEE J. Emerg. Sel. Topics Power Electron **4**, 707 (2016).
[2]H. Kambayashi, Y. Satoh, S. Ootomo, T. Kokawa, T. Nomura, S. Kato, and T.-S. P. Chow, Solid State Electron. **54**, 660 (2010).
[3]M. Wang, Y. Wang, C. Zhang, B. Xie, C. P. Wen, J. Wang, Y. Hao, W. Wu, K. J. Chen, and B. Shen, IEEE Trans. Electron Devices **61**, 2035 (2014).
[4]R. Vetury, N.-Q. Zhang, S. Keller, and U. K. Mishra, IEEE Trans. Electron Devices **48**, 560 (2001).
[5]P. B. Klein, J. A. Freitas, Jr, S. C. Binari, and A. E. Wickenden, Appl. Phys. Lett. **75**, 4016 (1999).
[6]M. Meneghini, N. Ronchi, A. Stocco, G. Meneghesso, U. K. Mishra, Y. Pei, and E. Zanoni, IEEE Trans. Electron Devices **58**, 2996 (2011).
[7]P. Hacke, T. Detchprohm, K. Hiramatsu, N. Sawaki, K. Tadatomo, and K. Miyake, J. Appl. Phys. **76**, 304 (1994).
[8]W. Götz, N. M. Johnson, H. Amano, and I. Akasaki, Appl. Phys. Lett. **65**, 463 (1994).
[9]P. Hacke, H. Nakayama, T. Detchprohm, K. Hiramatsu, and N. Sawaki, Appl. Phys. Lett. **68**, 1362 (1996).
[10]W. Götz, N. M. Johnson, and D. P. Bour, Appl. Phys. Lett. **68**, 3470 (1996).
[11]T. Mizutani, T. Okino, K. Kawada, Y. Ohno, S. Kishimoto, and K. Maezawa, Phys. Status Solidi A **200**, 195 (2003).
[12]Z.-Q. Fang, B. Claflin, and D. C. Look, J. Electron. Mater. **40**, 2337 (2011).
[13]M. El-Khatib, P. Ferrandis, E. Morvan, G. Guillot, and G. Bremond, Proc. SPIE **10532**, 1053225 (2018).
[14]Synopsys, TCAD tool, Sdevice User Guide N-2017.09.
[15]I. Vurgaftman and J. R. Meyer, J. Appl. Phys. **94**, 3675 (2003).
[16]D. C. Look and Z.-Q. Fang, Appl. Phys. Lett. **79**, 84 (2001).
[17]Z.-Q. Fang, D. C. Look, X.-L. Wang, J. Han, F. A. Khan, and I. Adesida, Appl. Phys. Lett. **82**, 1562 (2003).
[18]P. Ferrandis, M. Charles, Y. Baines, J. Buckley, G. Garnier, C. Gillot, and G. Reimbold, Jpn. J. Appl. Phys. **56**, 04CG01 (2017).
[19]W. I. Lee, T. C. Huang, J. D. Guo, and M. S. Feng, Appl. Phys. Lett. **67**, 1721 (1995).
[20]Z.-Q. Fang, D. C. Look, B. Claflin, S. Haffouz, H. Tang, and J. Webb, Phys. Status Solidi C **2**, 2757 (2005).
[21]A. Chini, M. Esposto, G. Meneghesso, and E. Zanoni, Electron. Lett. **45**, 426 (2009).
[22]A. Chini, V. Di Lecce, M. Esposto, G. Meneghesso, and E. Zanoni, in *Proceedings of the 4th European Microwave Integrated Circuits Conference* (EuMIC, 2009), p. 132; available at https://ieeexplore.ieee.org/xpl/mostRecentIssue.jsp?punumber=5286914.
[23]P. Ferrandis, M. Charles, C. Gillot, R. Escoffier, E. Morvan, A. Torres, and G. Reimbold, Microelectron. Eng. **178**, 158 (2017).
[24]F. D. Auret, S. A. Goodman, G. Myburg, S. E. Mohney, and J. M. de Lucca, Mater. Sci. Eng. B **82**, 102 (2001).
[25]D. Haase, M. Schmid, W. Kürner, A. Dörnen, V. Härle, F. Scholz, M. Burkard, and H. Schweizer, Appl. Phys. Lett. **69**, 2525 (1996).
[26]C. D. Wang, L. S. Yu, S. S. Lau, E. T. Yu, W. Kim, A. E. Botchkarev, and H. Morkoç, Appl. Phys. Lett. **72**, 1211 (1998).
[27]Z.-Q. Fang, D. C. Look, W. Kim, Z. Fan, A. Botchkarev, and H. Morkoç, Appl. Phys. Lett. **72**, 2277 (1998).
[28]Z.-Q. Fang, D. C. Look, P. Visconti, D.-F. Wang, C.-Z. Lu, F. Yun, H. Morkoç, S. S. Park, and K. Y. Lee, Appl. Phys. Lett. **78**, 2178 (2001).
[29]S. Chen, U. Honda, T. Shibata, T. Matsumura, Y. Tokuda, K. Ishikawa, M. Hori, H. Ueda, T. Uesugi, and T. Kachi, J. Appl. Phys. **112**, 053513 (2012).
[30]Z.-Q. Fang, G. Farlow, B. Claflin, and D. C. Look, in *Proceedings of the 13th International Conference on Semiconducting and Insulating Materials* (SIMC-XIII, 2004), pp. 29–36; available at https://ieeexplore.ieee.org/xpl/mostRecentIssue.jsp?punumber=10100#.
[31]F. D. Auret, S. A. Goodman, F. K. Koschnick, J.-M. Spaeth, B. Beaumont, and P. Gibart, Appl. Phys. Lett. **73**, 3745 (1998).